Vadose Zone Journal
ORIGINAL RESEARCH

Integration of Hard and Soft Data to Characterize Field-Scale Hydraulic Properties for Flow and Transport Studies

Eran Segal, Scott A. Bradford,* Pete Shouse, Naftali Lazarovitch, and Dennis Corwin

Field-scale flow and transport studies are frequently conducted to assess and quantify various environmental and agricultural scenarios. The utility of field-scale flow and transport studies, however, is frequently limited by our inability to characterize the heterogeneous distribution of hydraulic properties at these sites. In this study, we present an integrated approach, using both "hard" and "soft" data sets of field and laboratory scales in conjunction with pedotransfer functions, interpolation algorithm, and numerical modeling to characterize the hydraulic properties of the vadose zone. The approach is demonstrated at two 5- by 5-m field plots selected for research on the transport and fate of nutrients and pathogens. We used hard data to quantify the magnitude of the hydraulic properties at selected locations in these plots and included laboratory and field measurements of the hydraulic properties from undisturbed cores and the instantaneous profile method, respectively. More abundant soft data included inductive electromagnetic readings and approximate particle-size distribution information. The nearest neighbor interpolation algorithm was used to generate a heterogeneous realization of the saturated hydraulic conductivity on these plots. Numerical modeling of steady-state water infiltration and redistribution experiments was used to compare laboratory- and field-scale hydraulic properties and to refine our conceptual model of the vertical and lateral flow at this site. Good agreement between simulated and measured water contents and water pressure heads was obtained, indicating that field-scale hydraulic properties were accurately quantified for these conditions. This article provides a real-world example of how to combine information and approaches to tackle the difficult challenge of characterizing the hydraulic properties at a field site.

ABBREVIATIONS: EC_a, apparent soil electrical conductivity; EM, electromagnetic induction; ER, electrical resistivity; PSD, particle-size distribution; TDR, time domain reflectometry.

THE ABILITY TO accurately quantify water flow and solute transport in the field is necessary for a wide variety of applications concerned with water quantity and quality, as well as agricultural production. For example, at the field research site studied in this work, we need to accurately characterize the water flow behavior to understand, quantify, and manage the transport and fate of a conservative solute tracer, reactive nitrogen species, and microorganisms. Mathematical models that are used to simulate water flow require information on soil properties such as bulk density, soil porosity, soil water retention curves, saturated conductivity, and unsaturated conductivity relations (Scheidegger, 1957; Brooks and Corey, 1964; Lagerwerff et al., 1969; Mualem, 1976; van Genuchten, 1980). Field studies are generally conducted at designated plots without a full quantification of all the hydraulic properties of the soil profile or knowledge of the spatial variability of these properties (Thomasson et al., 2006). Hence, prediction of water flow processes is frequently hindered by our inability to accurately quantify the variability of soil hydraulic properties (Nielsen et al., 1973). These limitations become more significant when field plot experiments are chosen to represent the whole field or a large area (Kutilek and Nielsen, 1994). Variability in hydraulic properties occurs both horizontally in the field plane and vertically with soil profile depth, but is typically much more pronounced in the vertical direction (Vereecken et al., 2007). This variability occurs as result of differences in the factors that influence soil genesis and formation (Birkeland, 1984).

Several investigators have attempted to characterize field sites for flow and transport studies (Wierenga et al., 1991; Hills et al., 1991; Lehmann and Ackerer, 1997; Abbaspour et al., 2000; Zhang et al., 2004). Direct measurement of hydraulic properties may be made in the field or on samples that are taken to the laboratory. A variety of protocols have been developed for this purpose that invoke different simplifying assumptions and consider various sample sizes (Watson, 1966; Green et al., 1986; Klute, 1986; Klute and Dirksen, 1986; Reynolds and Elrick, 1991; Zhang et al., 2004). Direct measurement generally provides the best available determination of hydraulic property values and is therefore referred to in this manuscript as hard data. Because direct measurement of hydraulic properties is frequently time consuming, labor intensive, costly, and perturbs or destructively samples the system, only a limited number of measurements may be taken. As a result, a variety of indirect approaches have been developed to estimate hydraulic properties from other available information that is statistically correlated to soil properties and

E. Segal, Dep. of Environmental Sciences, Univ. of California, Riverside, CA 92521; S.A. Bradford, P. Shouse, and D. Corwin, USDA-ARS, U.S. Salinity Lab., Riverside, CA 92507; N. Lazarovitch, Ben-Gurion Univ. of the Negev, Israel. Received 8 May 2007. *Corresponding author (sbradford@ussl.ars.usda.gov).

Vadose Zone J. 7:878–889
doi:10.2136/vzj2007.0090

is easier to measure and–or more abundant. Indirect estimates of hydraulic properties are generally of lower quality and confidence than direct measurements, so these estimates will be referred to in this manuscript as soft data. Below we briefly review commonly employed methods to directly measure or indirectly estimate soil hydraulic properties.

Traditional approaches for directly measuring soil hydraulic properties in the field (hard data) include the use of tension infiltrometers (Reynolds and Elrick, 1991, Reynolds et al., 2000); double-ring infiltrometers (Bower, 1986); and the instantaneous profile method (Watson, 1966). The instantaneous profile method has been commonly applied to characterize field-scale hydraulic properties (Nielsen et al., 1973). Limitations of this method were discussed in Baker et al. (1974) and Flühler et al. (1976) and include the necessity of a large experimental plot that eliminates the boundary effect, a homogenous soil profile, and continuous data acquisition. Undisturbed core samples are also frequently taken from the field (Klute and Dirksen, 1986) and their soil hydraulic properties are determined in the laboratory (hard data). Laboratory methods are commonly employed on core samples to directly determine bulk density, porosity, water retention curves, saturated conductivity, and unsaturated conductivity relations (Grossman and Reinsch, 2002; Flint and Flint, 2002; Dane and Hopmans, 2002).

Indirect methods to characterize field-scale variability in soil hydraulic properties sometimes rely on measured particle-size distribution (PSD) information and soil bulk density of soil samples (Hillel, 1980). For example, pedotransfer functions and databases have been developed to predict water retention curves from this information (Schaap et al., 2001). Furthermore, unsaturated conductivity relations are frequently estimated from water retention curves using pore size distribution models (Brooks and Corey, 1964; Mualem, 1976; van Genuchten, 1980; Arya et al., 1999; Rajkai and Varallyay, 1992).

A variety of nondestructive methods can quantify large-scale trends in soil stratigraphy and other soil properties, including: seismic (Baker et al., 1999), ground penetrating radar (Davis and Annan, 1989; Inman et al., 2002; Huisman et al., 2003), electrical resistivity (ER) tomography (Daily et al., 2004); and electromagnetic induction (EM) (Corwin, 2005). Electromagnetic induction and electrical resistivity are both reliable methods for measuring apparent soil electrical conductivity (EC_a), but EM does not suffer from the problem of probe-to-soil contact that can occur with ER in dry or stony soils (Rhoades, 1993; Corwin and Lesch, 2003, 2005a). The value of the EC_a is influenced by soil solution salinity, water content, soil texture, bulk density, clay mineralogy, and organic matter content (Corwin and Lesch, 2005a). Geospatial measurements of EC_a enable one to estimate the spatial variability of texture (soft data) for the near surface (100–150 cm thickness) soil profile when texture is strongly correlated to EC_a, which often occurs when soil salinity and organic matter levels are low and are not the properties dominating the EC_a measurement (Corwin and Lesch, 2003, 2005a; Corwin, 2005).

The spatial variability of measured (hard data) or estimated (soft data) soil hydraulic properties may also be quantified using semivariograms. A variety of geostatistical algorithms have been developed to use semivariogram information to estimate (interpolated soft data) properties at other locations from a limited number of measured data points (Goovaerts, 1999). Application of such approaches to estimate soil hydraulic properties in the field is complicated by the fact that multiple parameters on different support scales need to be known. In such cases, scaling approaches are sometimes applied to relate different soil hydraulic properties to each other (Hopmans et al., 2002; Vereecken et al., 2007). Despite these advances, the use of measurements to predict field-scale soil hydraulic properties has been reported to be limited in many instances due in part to the relatively low sampling density of collected data in most instances (Jury and Horton, 2004).

Mathematical models used to simulate unsaturated water flow may also be used to estimate soil hydraulic properties, to study water flow, and–or to infer the implications of variability in soil hydraulic properties (Šimůnek et al., 1999). For example, soil hydraulic property parameters may be systematically adjusted to minimize the deviation between available experimental data and output of numerical models that simulate the relevant flow problem (Romano, 1993; Šimůnek et al., 1998). Conversely, numerical models may be used to study the implications of a given realization of soil hydraulic properties on water flow (the forward problem), or to study the influence of uncertainty in estimates of soil hydraulic properties using various Monte Carlo or stochastic approaches (Russo and Bresler, 1981). Vereecken et al. (2007) provided a recent review of various approaches to upscale hydraulic properties and water flow processes in heterogeneous soils.

The overall objective of this paper is to use available hard and soft data, and interpolation and modeling tools to characterize the soil hydraulic properties at a field-scale study site. Other researchers have used both hard and soft data to characterize the hydraulic properties of the vadose zone (Hubbard et al., 2001; Grote et al., 2003; Kowalsky et al., 2004, 2005; Lunt et al., 2005; Hou and Rubin, 2005). However, these studies have been limited to only some of the relevant hydraulic properties (water content, saturated conductivity, or permeability). The main contribution of this work is the use of a larger number of methods to determine a wider range of relevant hydraulic properties in the field, and the extensive refinement and validation of these hydraulic properties with laboratory and field measurements, and computer modeling. The following specific questions are addressed in this research: Are estimates of spatially variable soil hydraulic properties from soft data consistent with measured hard data? Does the integration of hard and soft data provide an improved ability to predict water flow in the field? How can we incorporate data from different spatial scales to characterize a field site?

Materials and Methods

Approach to Site Characterization

Figure 1 presents a flow chart illustrating the sequence of steps that are used to characterize a field site for flow and transport, as well as the methods and data types that were used in our particular application. Data type—soft data (S) and hard data (H)—reflects the level of confidence and accuracy of the collected data. The level of information needed to characterize a field plot depends on the application. The current research site is designed to study the transport and fate of nutrients and pathogenic microorganisms through the soil profile. This application requires a high level of confidence in water flow behavior and,

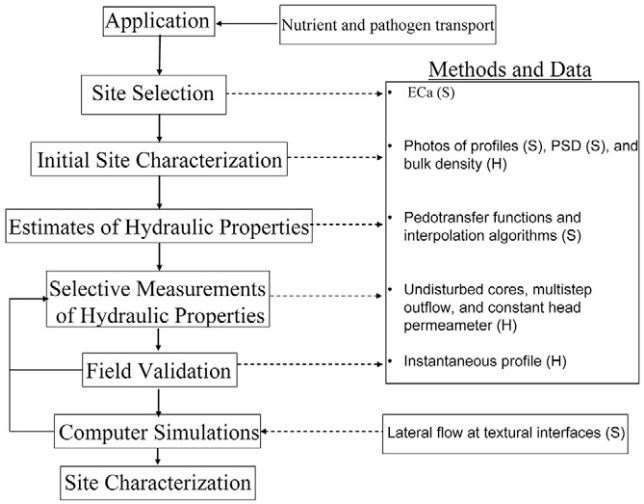

FIG. 1. A flow chart illustrating the sequence of steps that are used to characterize a field-site for flow and transport, as well as the methods and data types that were used in our particular application. Data type, soft data (S) and hard data (H), reflect the level of confidence and accuracy of the collected data. (PSD, particle-size distribution).

therefore, detailed information on the soil hydraulic properties. The first phase of our approach is site selection. Since the transport and fate of nutrients and microorganisms in the vadose zone are very complex processes (Bradford et al., 2008), measurements of the apparent soil electrical conductivity were used to select a highly uniform location within the 4-ha field to reduce the level of complexity and uncertainty. Obviously, alternative applications may lead to different criteria that will guide the site selection (e.g., locations of the greatest soil heterogeneity). The second phase of our approach involves an initial site characterization to identify the soil stratigraphy, approximate particle-size distribution, and bulk density information on soil cores and pits. The time-consuming and costly analysis of fundamental properties in the traditional way may not be practical. Soft data was therefore predominantly used in this phase. In the third stage, pedotransfer functions and interpolation algorithms are used to generate an initial conceptual model about the soil profile, including initial estimates of hydraulic properties. This conceptual model guides the selection location for undisturbed cores that capture the dominant water flow behavior under study. The hydraulic properties of undisturbed core samples are subsequently measured in the laboratory and used to further refine the conceptual model of the site hydraulic properties. The next phase of site characterization is field validation of the conceptual model of the soil hydraulic properties. Steady and transient water flow experiments are used to ensure good agreement between measured and simulated (numerical or analytical computer simulations) water flow data. Feedback between field experiments and computer simulations identifies locations in the field where additional measurements or computer simulations are needed to improve the conceptual model and understanding of the site. Below we discuss the various methods and computer simulations used in our application.

Field

A mobile remote electromagnetic induction sensor system (Geonics EM-38DD; Geonics Limited, Mississauga, Ontario, Canada) was used to measure EC_a (Corwin and Lesch, 2005a) across a 4-ha field. This system includes two EM-38 units synchronized to operate simultaneously, enabling measurements of both vertical and horizontal dipole conductivity. Data was collected following the protocols of Corwin and Lesch (2005b) to generate an approximately 5- by 5-m grid EC_a map of our field site. The map coordinates were determined using a global positioning system.

Selection of our experimental field plot for nitrate and pathogen transport studies was based on the generated EC_a map discussed above. The agricultural field in San Jacinto, CA (33°50′22″ N, 117°00′46″ W) was chosen for this purpose because it was associated with minimal spatial variability in EC_a readings, which implies relatively low heterogeneity in soil texture. The experimental plot is located next to a dry riverbed and has a shallow perched water table at a depth of –220 cm. This experimental site consists of two 5- by 5-m plots (Fig. 2). At the corners of each plot, a backhoe was used to expose the soil profile and to install 120-cm-diam. by 220-cm-long culvert pipes vertically into the soil (Fig. 2, circles marked with letters). Soil profiles in each culvert pipe hole were photographed and notes on soil stratification were taken before installing each culvert pipe. The culvert pipes were instrumented with six tensiometers to measure the soil water pressure with depth increments of 30 cm. The tensiometers, 90 cm in length, were installed horizontally from the culvert pipe into the undisturbed soil profile. The staggered configuration of the tensiometers was selected to minimize the potential for preferential flow and potential interference from other sensors, and to maximize the area of the profile that was sampled. The arc in Fig. 2 represents the area of water potential sampling. Pressure transducers (MPX2100DP, Motorola, Denver, CO) and a data logger (CR7, Campbell Scientific, Inc., Logan, UT) recorded the tensiometer readings every 15 min. Five neutron access tubes (220 cm long) were installed vertically on each plot (Fig. 2, circles marked with Roman numerals). The water content with depth at desired times was determined using a neutron probe (503-DRHYDROPROBE, CPN, Martinez, CA) and an established calibration curve in this soil profile.

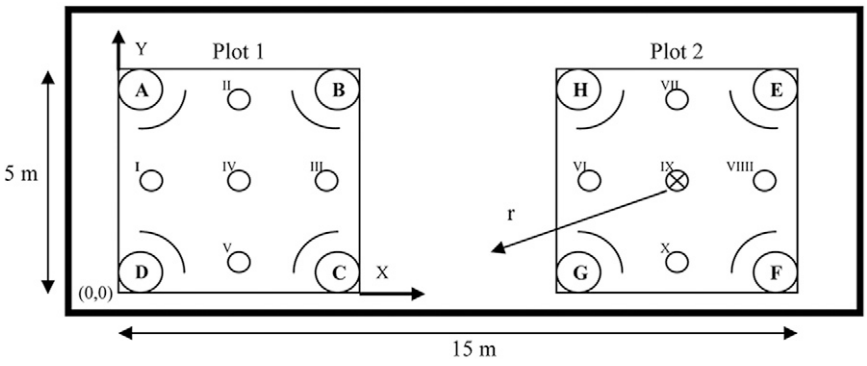

FIG. 2. A schematic of the field site. Squares represent two 5- by 5-m plots. Circles with letters are 220 cm in length vertical culvert pipes installed with six tensiometers. Circles with Roman numerals are vertical neutron probe access tubes. Arcs represent the area of water potential sampling. The crossed circle in the center of Plot 2 denotes the origin of a radial axis (*r*).

The instantaneous profile method (Watson, 1966) was used to evaluate the hydraulic conductivity of the upper 60 cm of the profile at the field site. This method uses simultaneous measurements of the volumetric water content (θ) and soil water pressure head (h) in a soil profile during the course of drainage to determine the hydraulic conductivity. The equation describing one-dimensional unsaturated flow of water during drainage subject to zero flow at the upper boundary is utilized for this purpose (Green et al., 1986):

$$K(\theta) = \frac{\int_0^{z_i} \frac{\partial \theta(z,t)}{\partial t} \mathrm{d}z}{\left.\frac{\partial \phi(z,t)}{\partial z}\right|_{z_i}} \qquad [1]$$

where K is the hydraulic conductivity (m s^{-1}), θ is volumetric water content (m^3 m^{-3}), ϕ is the total hydraulic head of the soil water (m), t is time (s), z is the vertical coordinate measured positive downward (m), and i is the depth index. Before initiating the drainage process, the soil profile was under a steady infiltration of 6 cm d^{-1} for 14 d. The water was uniformly applied to the plot surface using drip irrigation (Typhoon 630, Netafim, Fresno, CA) on a 0.4- by 0.4-m grid. The soil surface was covered with a black nylon tarp to avoid water evaporation during infiltration and drainage. The value of h (m) with depth was continuously monitored during drainage using tensiometers in the culvert pipes, and the θ distribution in the profile was measured daily with a Neutron probe. Equation [1] was used to calculate the unsaturated hydraulic conductivity based on these θ and h measurements.

An additional set of θ and h data was measured near saturation (h = 0 to −30 cm) during redistribution of water immediately after ponded infiltration ceased (Hillel, 1998). In this case, the value of θ was acquired using a time domain reflectometry (TDR) system (Trase system, Soilmoisture Equip. Corp., Santa Barbara, CA) as well as gravimetrically, and h was monitored with a tensiometer (Tensimeter, Soil Measurement Systems, Tucson, AZ).

Laboratory

Large permeability differences have been reported for undisturbed and repacked cores due to soil structure (Tuli et al., 2005). The undisturbed core method is the most common technique to estimate field soil hydraulic properties in the laboratory (Klute and Dirksen, 1986). Although this method is limited by sampling size and the potential for flow along the core wall (Cameron et al., 1990), it is considered to be a benchmark for evaluating other methods (Reynolds et al., 2000). Undisturbed cores from the experimental site were collected for measurements of bulk density (ρ_b) and hydraulic properties. These cores were collected using a soil core sampler (Soilmoisture Equip. Corp., Santa Barbara, CA) and a drilling rig for deeper depths. Samples were collected vertically every 30 cm (soil surface to −150 cm), and locations were on the boundaries of each plot next to the neutron access tubes (I, II, V, VII, VIII, and X in Fig. 2). Undisturbed cores from two locations (I and X in Fig. 2) and five depths (−30, −60, −90, −120, and −150 cm) were used for retention curve and saturated hydraulic conductivity (K_s) measurements.

The soil bulk density was determined using the known volume sample method (Blake and Hartage, 1986). The primary drainage branch of the retention curve from each undisturbed core (between −1 and −333 cm of pressure head) was measured using the Tempe cell (multistep outflow) technique (Reginato and van Bavel, 1962; Klute, 1986; Eching et al., 1994). A semiautomatic Tempe cell apparatus was used to control and record the measurement of 10 Tempe cells that were run in parallel. The water contents at lower water pressure heads were measured using a pressure plate apparatus (Soilmoisture Equip. Corp., Santa Barbara, CA) according to the approach outlined by Richards (1965).

A constant head permeameter (Klute and Dirksen, 1986) was used to measure K_s on each core. A standard solution (calcium chloride, 0.003 M) was allowed to infiltrate for 24 h at a constant positive head of 5 cm that was applied using a mariotte bottle. After reaching steady-state flow conditions, the flow rate was determined by weighing the effluent samples that were collected over regular time intervals. The average K_s value was calculated from these measurements.

The retention data were fitted to the Mualem–van Genuchten hydraulic model using the RETC computer code (van Genuchten et al., 1991). The retention parameters of the model and the saturated hydraulic conductivity were used to estimate the unsaturated hydraulic conductivity relation. The Mualem–van Genuchten hydraulic model (Mualem, 1976; van Genuchten, 1980) describes the nonlinear relations in porous media between the effective water saturation (S_e), soil water pressure head (h), and hydraulic conductivity (K) as

$$\begin{aligned} S_e &= \frac{\theta - \theta_r}{\theta_s - \theta_r} \\ S_e(h) &= 1 \qquad\qquad h \geq 0 \\ S_e(h) &= \frac{1}{\left(1 + |\alpha h|^n\right)^m} \quad h < 0;\ \text{where } m = 1 - \frac{1}{n} \\ K(S_e) &= K_s S_e^{0.5}\left[1 - \left(1 - S_e^{1/m}\right)^m\right]^2 \end{aligned} \qquad [2]$$

where θ_s, θ_r, and θ are the saturated, residual and actual volumetric water content, respectively (m^3 m^{-3}), h is the soil water pressure head (m), K_s is the saturated hydraulic conductivity (m s^{-1}), and α (m^{-1}), n, and m are soil-specific water retention curve parameters.

The particle-size distribution is one of the fundamental properties of mineral soils. It can be described by three parameters: median particle size, uniformity coefficient, and soil texture (Gee and Bauder, 1986; Hillel, 1980). The soil cores from the neutron access tubes installation in the field site (Fig. 2) were collected and cut to 15-cm intervals for particle-size distribution analysis. Each segment was thoroughly mixed, and a 1-g sample was dispersed in 50 g L^{-1} of hexametaphosphate solution before analysis with a laser light scattering particle-size distribution analyzer (LA 930, Horiba Ltd., Kyoto, Japan). The soil texture, median particle size (d_{50}), and the Hazen uniformity coefficient (calculated as the ratio of d_{60} and d_{10}, where d_{60} and d_{10} are the 60th and 10th percentile of the cumulative percentage undersize by volume of the soil sample, respectively) were determined for each sample. The laser scattering technique is a semiquantitative tool to measure the PSD of many soil samples in a short time (Eshel et al., 2004), and it is a practical tool to analyze trends in the profile's PSD.

Information from the particle-size distribution has been used to estimate soil hydraulic properties (Arya et al., 1999; Rajkai

and Varallyay, 1992; Schaap et al., 2001). Schaap et al. (2001) presented a computer program, ROSETTA, that estimates the hydraulic properties of soils based on a large database of soil properties and pedotransfer functions. The collected PSD and bulk density information served as input for the ROSETTA program to estimate a higher density of "soft data" soil hydraulic properties. Particle-size distribution data were used to estimate K_s based on the distribution of sand, silt, and clay particles in the soil profiles. Since the lower soil profile consisted of multiple layers of different texture, the effective vertical saturated conductivity (K_s^v) was calculated based on the harmonic mean of the K_s for the individual layers (K_{sj}) as:

$$K_s^v = \frac{\sum_{j=1}^{n} L_j}{\sum_{j=1}^{n} \frac{L_j}{K_{sj}}} \quad [3]$$

where L is the layer thickness (m) and j is the layer index ($j = 1 \ldots n$).

Simulations

Numerical modeling is the most practical tool for simulating water flow in the field due to the high nonlinearity of Richards' equation under unsaturated flow conditions and the heterogeneity of the soil profiles. The HYDRUS-2D code (Šimůnek et al., 1999) is a numerical model for simulating water flow, and solute and heat transport in variably saturated porous media. The governing flow equation for axisymmetrical three-dimensional Darcian flow in a variably saturated isotropic porous medium is given by the following mixed form of Richards' equation:

$$\frac{\partial \theta}{\partial t} = \frac{1}{r}\frac{\partial}{\partial r}\left(rK(h)\frac{\partial h}{\partial r}\right) + \frac{\partial}{\partial z}\left[K(h)\frac{\partial h}{\partial z}\right] - \frac{\partial K(h)}{\partial z} \quad [4]$$

where r is a radial coordinate (m).

The HYDRUS-2D code with an axisymmetric geometry was used to simulate the water flow in the upper profile during steady-state infiltration and drainage experiments on Field Plot 2. Based on the plot size and the profile depth, the simulation domain was selected to be 90-cm thick (z) by 500 cm in the radial direction (r). The crossed circle in Fig. 2 is the center location of the radial axis, whereas the X, Y, and Z (depth) axes in this figure are for the Cartesian coordinate system. The simulated profile consisted of three soil textural layers, which corresponded to the texture estimated from the PSD and bulk density data. The first layer was sandy loam and was located between 0 to –70 cm depth followed by a 10-cm thick coarse sand layer, and then a 10-cm thick finer silt loam layer. The hydraulic properties of each layer in the profile were set to measured properties from undisturbed cores samples that were taken from each layer or estimated using PSD and bulk density data in conjunction with ROSETTA.

Measured data and model output during steady-state infiltration and subsequent drainage were compared for 15 d. The top boundary along $r \leq 250$ cm was set equal to a variable flux boundary condition; with a flux of 6 cm d^{-1} over 6 d of steady-state infiltration and a zero flux during the following 15 d of drainage, since the soil surface was covered during the experiments. For $r > 250$ cm, the upper boundary was no flow. The lower boundary was set to variable water pressure head at $r \leq 250$ cm and free drainage through $r > 250$ cm. The variable water pressure head at the lower boundary was based on field measurements at that depth (–90 cm) during steady infiltration and drainage processes. Since the side was not affected by the water flow, it was set to be a no flow boundary. The initial water pressure head distribution was set as hydrostatic.

Additional simulations were conducted for Plot 2 to determine the lateral water flux ($q_{lateral}$) that may occur directly above or through the sand layer at a depth of –70 to –80 cm relative to the vertical surface water flux ($q_{surface}$). The top boundary along $r \leq 250$ cm was set equal to $q_{surface}$, whereas for $r > 250$ cm the upper boundary was no flow. The lower boundary was set to free drainage. Two subdomains were defined in the model for mass balance considerations: an internal soil volume ($0 < r \leq 250$ cm) and external soil volume ($250 < r \leq 500$ cm). The intensity of the simulated surface water flux was varied between 0.5 to 20 cm d^{-1} and $q_{lateral}$ was calculated from the following set of equations that were based on the subdomain's mass balance information:

$$\begin{aligned} \Delta V_{int} &= V_{surface} - D_{int} - V_{lateral} \\ \Delta V_{ext} &= V_{lateral} - D_{ext} \\ D_{total} &= D_{int} + D_{ext} \\ &\text{where} \\ V_{surface} &= q_{surface} A_{surface} \Delta t \\ V_{lateral} &= q_{lateral} A_{lateral} \Delta t \end{aligned} \quad [5]$$

Here $A_{surface}$ is the area (cm^2) for surface water flow into the internal subdomain, $A_{lateral}$ is the area (cm^2) for lateral water flow from the internal to the external subdomain, $V_{surface}$ is the cumulative water volume (cm^3) that enters the internal subdomain at the surface, $V_{lateral}$ is the cumulative water volume (cm^3) that leaves the internal subdomain laterally to the external subdomain, and D_{total} D_{int}, and D_{ext} are the cumulative drainage water volume (cm^3) in the total, internal, and external domains, respectively. The quantities ΔV_{int} and ΔV_{ext} denote the soil water volume (cm^3) changes in the internal and external domains, respectively. Values of $V_{surface}$, D_{total}, ΔV_{int}, and ΔV_{ext} were calculated by HYDRUS over a specific time period (Δt).

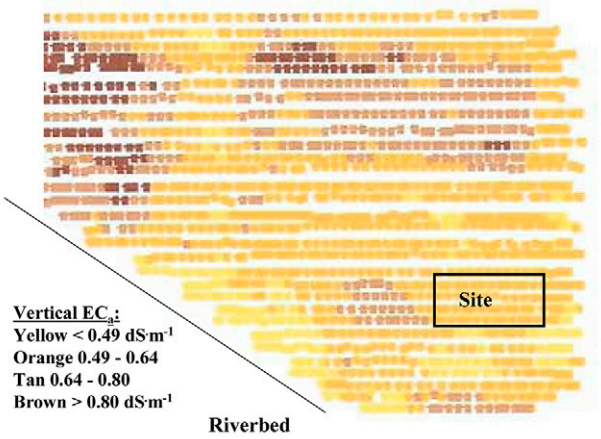

FIG. 3. A 4-ha map of the vertical component of the apparent soil electrical conductivity in the field as measured using a mobile remote electromagnetic induction sensor system on a 5- by 5-m grid.

Results and Discussion

Soft Data

In this section we discuss the use of soft data to select a location for flow and transport studies and to develop a conceptual model of the soil hydraulic properties at this field site.

Electromagnetic induction technology was used to quantify the field spatial variability of EC_a. Although soil heterogeneity and spatial variability are inherent in field-scale studies, reducing the soil textural variability is sometimes essential for managing and interpreting flow and transport studies. Figure 3 shows a map of the vertical component of EC_a. The experimental study site was selected from this soft EC_a data to be located in a "relatively uniform" section of the field with low EC_a values (coarser textured material).

Our initial conceptual model of the soil profile stratigraphy at the experimental site was developed from photographic information. Figure 4a provides a representative photo of Pit C, which was taken just before installation of the culvert pipe. A uniform layer of sandy loam was situated from the surface down to a depth of about −70 cm, followed by a white sand layer (−70 to −80 cm). A finer textured clayey lens with variable thickness was found below the sandy layer. The deeper profile (less than −80 cm) was characterized by a sandy loam layer, which incorporated various sand and clay lenses at different depths. This profile description was also consistent with measured soil bulk densities (hard data) that are presented in Fig. 4b. The bulk density data represent an average of six locations (I, II, V, VII, VIII, and X), and the horizontal bars provide the standard deviations. The bulk density values at the upper sandy loam layer were around 1.35 g cm^{-3} and exhibited low variability. The sandy layer had a high bulk density of 1.55 g cm^{-3}. Values of the bulk density from the lower profile were affected by the sandy and clayey lenses at different locations and therefore produced higher variability in these measurements.

Soft particle-size distribution data (laser light scattering) were collected at multiple locations and depths to rapidly evaluate the spatial variability of soil texture and K_s with depth at the experimental site. Figure 5 presents the PSD data at the location of neutron access tubes nos. I, V, IX, and X. In this figure the median grain size (d_{50}) are plotted with depth in 15-cm intervals. The horizontal bars on d_{50} are defined herein by values of d_{10} and d_{60} (used to determine the Hazen uniformity coefficient as d_{60}/d_{10}) and provide an estimate of the spread in the particle-size distribution. The radial distance for each location that is provided in the figure was measured from neutron access tube IX. While the upper layer (0 to −70 cm) has highly uniform d_{50} values of approximately 50 μm, the sandy layer (−70 to −80 cm) has d_{50} values that ranged from 150 to 250 μm with low uniformity. Although the fine-textured lenses and sand layers below a depth of −70 to −80 cm were not visible in each profile due to the sampling method (averaging 15 cm core), variability in d_{50} values indicated their existence and the location of these layers. For example, lower d_{50} values were measured in Profile IX (r = 0 m) directly below the sandy layer (−70 to −80 cm) and indicated the existence of a fine-textured lens. High d_{50} values were measured in Profiles I and X (r = 12.5 m, 2.5 m) at locations that were associated with sand layers.

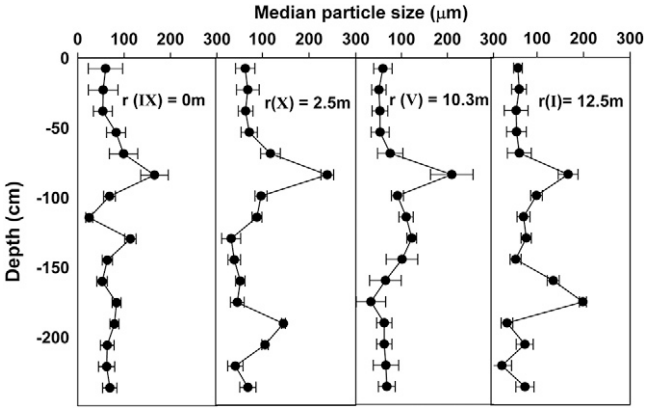

FIG. 5. Median size of soil particles in 15-cm intervals from Locations I, V, IX, and X. The horizontal bars on these measurements are values of d_{10} and d_{60} used to calculate the Hazen uniformity coefficient.

The PSD (soft data) and bulk density data from locations I to V were used in conjunction with the ROSETTA program to estimate values of K_s at sampled locations. The nearest neighbor algorithm was then used to interpolation values of K_s at other locations that were not sampled. Figure 6 presents the estimated

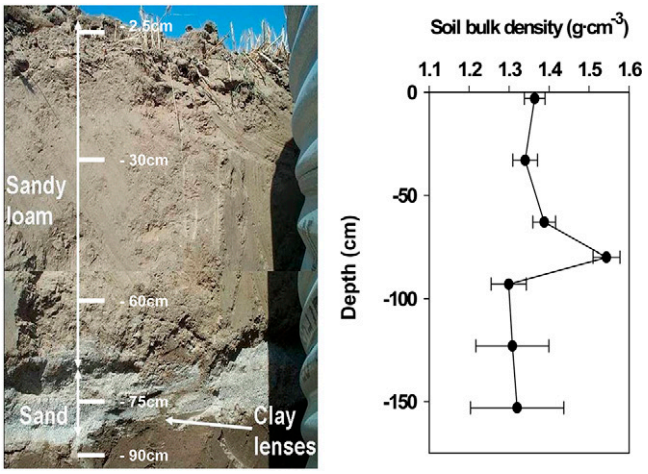

FIG. 4. (a) A photo of the upper soil profile (Pit C). (b) Soil bulk density measurements at six locations (I, II, V, VII, VIII, and X); the horizontal bars provide the standard deviations.

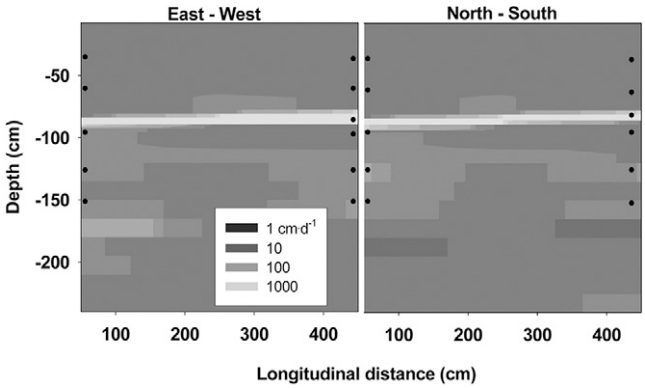

FIG. 6. North–south and east–west transects of estimated values (soft data) of K_s on Plot 1. These transects were generated from a three-dimensional map of K_s that was estimated using particle-size distribution and bulk density data from Locations I–V using ROSETTA and the nearest neighbor interpolation algorithm. Circles represent the undisturbed core sampling locations.

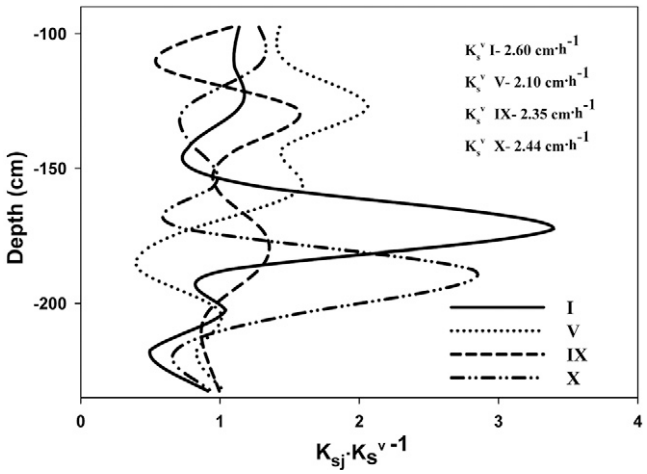

FIG. 7. A plot of the ratio of the harmonic mean of the saturated conductivity for the individual layer (K_{sj}) to the effective vertical saturated conductivity (K_s^v) for each layer in the lower section of the soil profile (−90 to −230 cm) at Locations I, V, IX, and X.

values of K_s on north–south and east–west transects of Plot 1. The dark uniform layer between the soil surface and −70 cm was the cultivated layer. The light-colored thin layer underneath the cultivated layer was the sandy layer (−70 to −80 cm). The lower soil profile (−80 cm to −210 cm) was scattered with multiple lenses of different texture. Dark colors represent fine-textured lenses, for instance on the north side at −180 cm. Conversely, light-colored spots are coarse-textured soils, such as on the east side at −170 cm. Both plots showed a coarse layer crossing the plot at around −120 cm.

The data presented in Fig. 6 can be further analyzed in terms of one-dimensional vertical conductivity. Figure 7 presents a plot of K_{sj}/K_s^v for each layer in the lower section of the soil profile (−90 to −230 cm) at locations I, V, IX, and X. These values of K_{sj}/K_s^v demonstrate the spatial variability and heterogeneity of the lower profile. Each profile consisted of multiple layers and values of K_{sj} varied by a factor of 5. The higher K_{sj}/K_s^v values were associated with sandy layers, whereas lower values were finer textural soils. The K_s^v of each location, however, were very similar (Fig. 7).

Two approaches were presented above to analyze the heterogeneous hydraulic properties in the lower portion of the soil profile at the experiment site using available (soft) PSD data. The first approach considered three-dimensional information on estimated K_s values to provide a more precise representation of water flow and solute transport (Fig. 6). The second approach considered the effective hydraulic properties with depth (Fig. 7). In this case, the analysis of estimated values of K_s generated similar values for K_s^v in the lower profile of the soil at four locations (I, V, IX, and X). The advantage of the first approach is the ability to deterministically model the water flow paths in the heterogeneous lower profile, but the database that is needed to generate the high resolution data set is not always available. Moreover, the predicted soil hydraulic properties might not be sufficiently accurate or collected over a fine enough scale to fully characterize the water flow pathways in this situation deterministically (Kutilek and Nielsen, 1994). Alternatively, geostatistical approaches may be used to quantify variability in soil hydraulic properties from measured horizontal and vertical correlation structures in the hydraulic properties (Russo and Bresler, 1981; Jury, 1985; Ünlü et al., 1990; Mohanty et al., 1994). For instance, the estimated values of K_s presented in Fig. 6 are one possible realization of the variability of K_s in the soil profile.

Hard Data

The soft data discussed above provided valuable information that was used to guide our strategy for collecting additional hard data in the field and the laboratory. This hard data was used to further refine our conceptual model and to improve our quantification of key soil hydraulic properties at the field site. Furthermore, comparison of field and laboratory data was used to identify potential limitations of the various types of hard data, and to assess the predicted hydraulic properties that were estimated from the soft data.

Undisturbed cores were collected for hydraulic property analysis at several locations in the root zone (0 to −70 cm), at the capillary barrier (sand layer), and in the lower profile (below −80 cm). These sampling locations were chosen to improve our understanding of water flow in areas of the site where distinct differences in estimated soil hydraulic properties were identified (soft data shown in Fig. 4–6). Figure 8 presents the measured laboratory soil water retention curve and K_s information as a

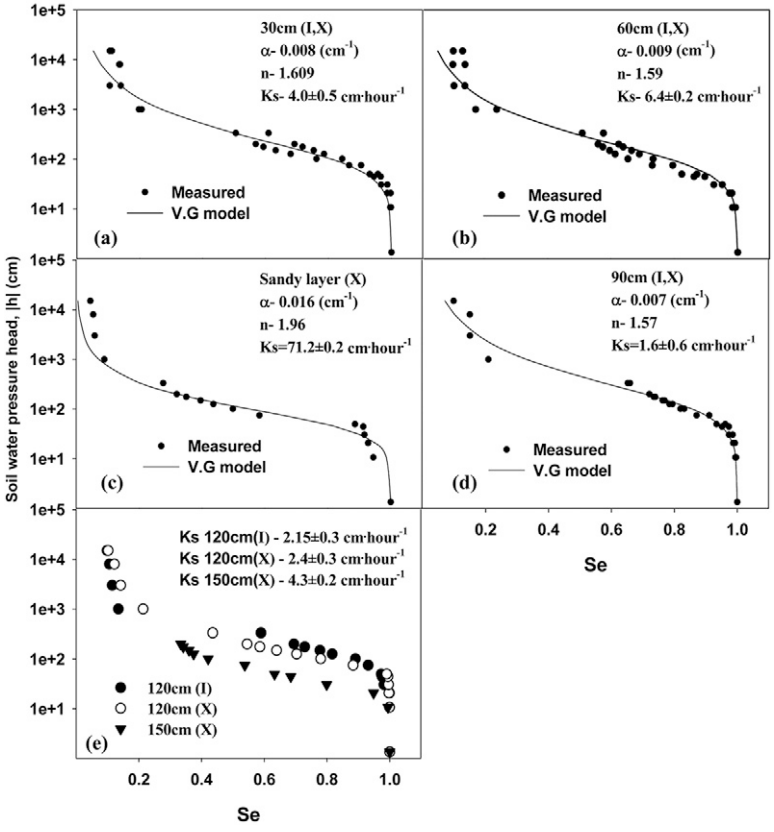

FIG. 8. Water retention curves (effective water saturation [S_e] as a function of water pressure head [h]) and saturated hydraulic conductivity (K_s) as a function of depth for Locations X and I and Plot 2. The data were acquired by the Tempe cell technique (a–e). Measured data (points) and the van Genuchten (1980) model (V.G. model, solid line) are shown, with retention curve parameters α and n given in the legend.

function of depth for Locations I and X. This hard data (Fig. 8a-e) was acquired using the multistep outflow technique. The measured data (points) and fitted hydraulic model (solid line) are depicted for specified depths. The corresponding retention curve parameters α and n of the Mualem–van Genuchten hydraulic model are also provided on each chart (Fig. 8a–d). The hydraulic properties generated from the laboratory methods reflected the different soil textures that were identified by the bulk density and PSD information presented in Fig. 4 and 5, respectively. The upper 0 to –70 cm was a spatially homogenous layer with similar water retention properties (Fig. 8a and b). The sandy layer located around –70 to –80 cm was distinguished by lower water holding capacity at a given soil water pressure (Fig. 8c). The lower profile was heterogeneous below –90 cm and the water retention properties, therefore, varied with depth and space (Fig. 8e). The K_s values in the upper soil profile (0 to –70 cm, Fig. 8a and b) were two times higher than in the lower profile (–90 to –150 cm, Fig. 8d and e). The K_s of the sandy layer (–70 to –80 cm, Fig. 8c) was more than one order of magnitude greater than the upper soil profile (0 to –70 cm, Fig. 8a and b).

Figure 9 presents field measurements of water content (Fig. 9a) and water pressure head (Fig. 9b) as a function of depth at Plot 2 during steady-state infiltration (time = 0) and drainage (time > 0). This data was an average value from culvert pipes E, F, G, and H, and the horizontal bars in this figure are the standard deviations. The initial θ and h values reflected the steady infiltration water flow pattern of the profile, before the drainage process. The constant lower θ values at approximately –90 and –180 cm were due to the presence of the sandy layers. The positive h value during time zero at –150 cm was attributed to perched water, a result of a fine-textured layer located at this depth, which has a lower value of K_s than the steady infiltration rate. Over time both θ and h decreased during drainage. Measurements of θ, however, were constant next to the water table at a depth of –220 cm.

The data collected from Plot 2 shown in Fig. 9 was analyzed with Eq. [2] (instantaneous profile method) to determine $K(S_e)$ at depths of –30 and –60 cm. Analysis of the entire profile with this method was not possible due to the layering at the site, which violated an assumption of this approach (no lateral flow). Figure 10 presents a plot of these calculated values of K as a function of S_e (full circles). This figure also includes Mualem–van Genuchten model (Eq. [3]) values of $K(S_e)$ that were determined from the laboratory multistep outflow experiments of the undisturbed

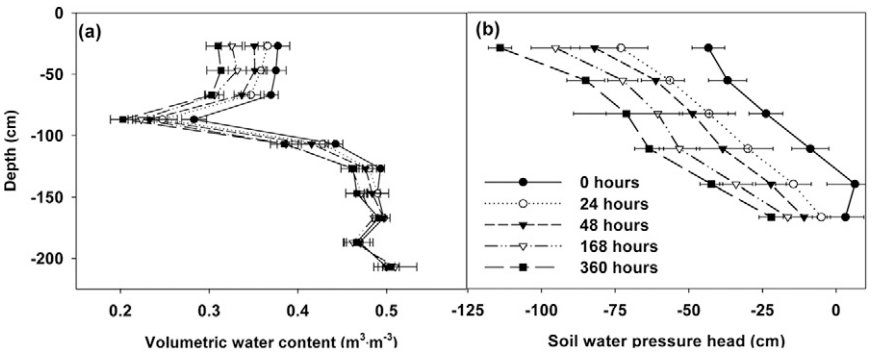

FIG. 9. (a) Water content and (b) water pressure head as a function of depth during steady state infiltration and drainage of the field soil profile. Data are an average value from Pits E, F, G, and H; horizontal bars are standard deviations.

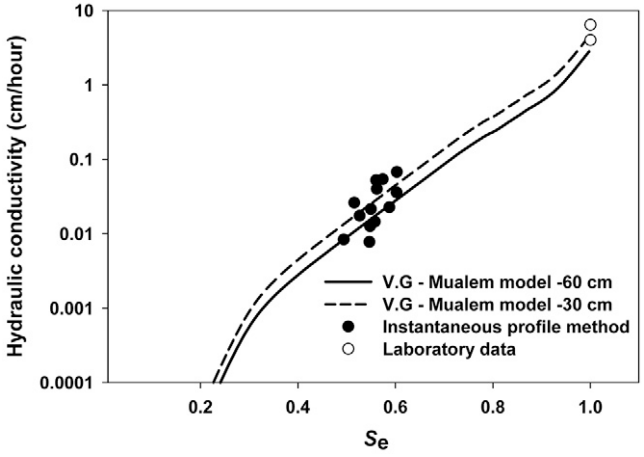

FIG. 10. A plot of hydraulic conductivity (K) versus effective water saturation (S_e) for the sandy loam layer at –30 and –60 cm. The solid lines are simulated data from the Mualem–van Genuchten hydraulic model (van Genuchten, 1980) based on undisturbed core data. The solid circles are calculated data based on the instantaneous profile method, and the open circles are laboratory measurements of K_s.

cores (Fig. 8) for the sandy loam layer at depths of –30 and –60 cm (lines). The K_s values (open circles) were measured in the laboratory. Although the range of θ measurements was rather limited (because drainage was inhibited by the shallow water table), good agreement was found between simulated laboratory curves and data derived by direct field measurements. Hence, the laboratory outflow data provided a reasonable forecast of the actual field conductivity for this soil (Fig. 10).

Figure 11 presents laboratory and field measurement of both $h(\theta)$ and $h(S_e)$ data from the sandy loam layer (0 to –70 cm). Recall that laboratory water retention measurements were obtained on undisturbed core samples using the Tempe cell and pressure plate techniques, whereas the field measurements were obtained using tensiometers, neutron probe, TDR and gravimetric samples during the drainage profile experiments (Fig. 9). Field and laboratory values of $h(S_e)$ matched reasonably well. In contrast, field and laboratory values of $h(\theta)$ showed considerable dissimilarity and revealed limitations of using only lab information to describe field-scale hydraulic properties. Specifically, the values of θ near saturation were considerably smaller in the field than in the laboratory measurement. Assuming similar porosity of the soil under field and laboratory conditions (undisturbed soil cores), a potential explanation for this difference could be entrapped air in the field. In the laboratory, entrapped air is nearly absent due to the slow saturation of the core from the bottom, but cores were also likely to have artificial pores at the boundaries of the Tempe cell. Figure 11 also includes fitted retention model parameters to show that α and n were very similar for field and laboratory water retention curves.

Validation and Simulations

In this section we compare soft and hard estimates of hydraulic properties from several locations in the field. Numerical simulations

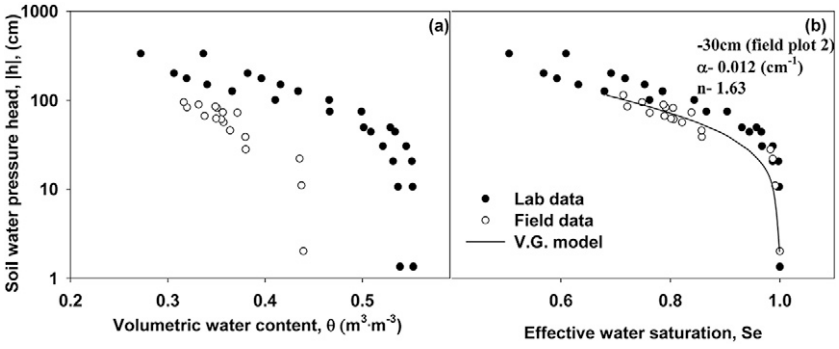

FIG. 11. Retention curve data, volumetric water content (θ), and effective water saturation (S_e) as a function of soil water pressure head (h) of the upper sandy loam layer. Lab (solid circles) refers to the multistep outflow technique and Field (open circles) refers to tensiometers and neutron probe or time domain reflectometry. Field data were fitted to the Mualem–van Genuchten hydraulic model (V.G. model, solid line).

were subsequently conducted to independently "validate" our field-scale hydraulic properties where possible and to further improve our understanding of water flow at specific locations in the field. Moreover, the reliability of using soft and hard data as input for simulations of water flow was demonstrated.

Table 1 presents a comparison between the hydraulic properties generated from soft and hard data. This information was obtained for three layers in the upper soil profile of the field site (0 to −70 cm; −70 to −80 cm; and −80 to −90 cm). In general, estimates of the hydraulic properties for the silt loam layer based on soft and hard data were very consistent. In contrast, estimates of the hydraulic properties based on soft data were poorer for the coarser textured sandy loam layer and especially the sand layer. In particular, estimation of K_s based on soft data underpredicted the hard data, and use of soft data produced higher estimated values of h (a lower capillary pressure) at a given value of S_e. A more rigorous statistical analysis of the hydraulic properties estimated from the hard and soft data was not attempted due to the limited number of hard data measurements.

The inverse procedures or scaling factors have commonly been used to characterize water flow behavior in the field (Vereecken et al., 2007; Jury and Horton, 2004; Hopmans et al., 2002; Thomasson et al., 2006). Conversely, we attempt to independently describe field-scale water flow using measured (hard data) or estimated (soft data) hydraulic properties in a numerical simulator. Figure 12 presents plots of observed and simulated values of h and S_e at a depth of −30 and −60 cm during steady infiltration and subsequent drainage. The steady infiltration data is given at time equal to zero and drainage occurred at later times for 360 h. The simulations employed hydraulic properties given in Table 1 that were measured (Fig. 12a) or estimated (Fig. 12b). A better agreement was found between measured and simulated values of S_e and h when using hard than soft data hydraulic properties (higher correlation coefficients, ρ). In general, simulations that employed hydraulic properties that were measured in the laboratory provided an excellent description of water flow during steady infiltration and drainage. This finding suggests that our site characterization approach gave an accurate description of water flow in the soil profile to at least a depth of around −70 cm. Also, a slightly better agreement was found between measured and simulated values of h (ρ of 0.989 and 0.962) than for S_e (ρ of 0.945 and 0.907). This difference may be related to the measurement methods. Water content was measured with a neutron probe, which averaged over a soil sphere of around 20–30 cm in diameter (Kutilek and Nielsen, 1994). In comparison, the soil water pressure head was measured with tensiometers that averaged over a smaller cylindrical soil volume of around 1 to 15 cm^3.

Figure 9 illustrates that water flow at the experimental plot is strongly influenced by the presence of the shallow water table at around −220 cm and a sand layer at a depth of −70 to −80 cm. The influence of the shallow water table is relatively easy to understand, as it produces persistently high values of θ in the lower portion of the soil profiles (see Fig. 9a) and restricts the minimum values of h and θ at the soil surface (see Fig. 9a,b). The potential influence of the sand layer (−70 to −80 cm) is more complicated to understand due to the potential for water flow to be diverted laterally both above and at the bottom of this layer. Lateral water flow above the sand layer may occur due to differences in the capillary properties of the upper sandy loam layer (0 to −70 cm) and the sand layer (i.e., a capillary barrier). Lateral water flow at the bottom of the sand layer may also occur as result of the higher permeability of the sand layer compared with the lower silt loam layer and clay lenses (less than −80 cm). Both of these lateral water flow processes are anticipated to be strong functions of the surface water infiltration rate and the water content of the profile. Numerical simulations were therefore conducted to improve our conceptual understanding of the influence of the surface water flux on water flow in the upper profile and the lateral water flux directly at or above the sand layer.

Figure 13 presents a plot of the ratio of the simulated lateral water flux through the plot's upper profile to the vertical surface water flux ($q_{lateral}/q_{surface}$) as a function of $q_{surface}$. Hydraulic

TABLE 1. The hydraulic properties of the three major layers in the upper soil profile of the field plot. Soft data were estimated from particle-size distribution and bulk density data using the ROSETTA program. Hard data were measured on undisturbed core samples using the multistep outflow, pressure plate, and constant head permeameter techniques or from time domain reflectometry readings in the field site.

Hydraulic property†	Layer 1: Sandy loam 0 to −70 cm		Layer 2: Sand −70 to −80 cm		Layer 3: Silt loam −80 to −90 cm	
	Soft data	Hard data	Soft data	Hard data	Soft data	Hard data
K_s (cm h^{-1})	1.95	5	9.25	71.2	1.4	1.6
θ_s	0.37	0.43	0.35	0.33	0.41	0.45
θ_r	0.033	0.03	0.04	0.01	0.056	0.04
α (cm^{-1})	0.018	0.0085	0.042	0.016	0.0047	0.007
n	1.45	1.6	2.41	1.96	1.70	1.57

† K_s, saturated hydraulic conductivity; θ_s, saturated volumetric water content; θ_r, residual volumetric water content; α and n, soil-specific water retention curve parameters.

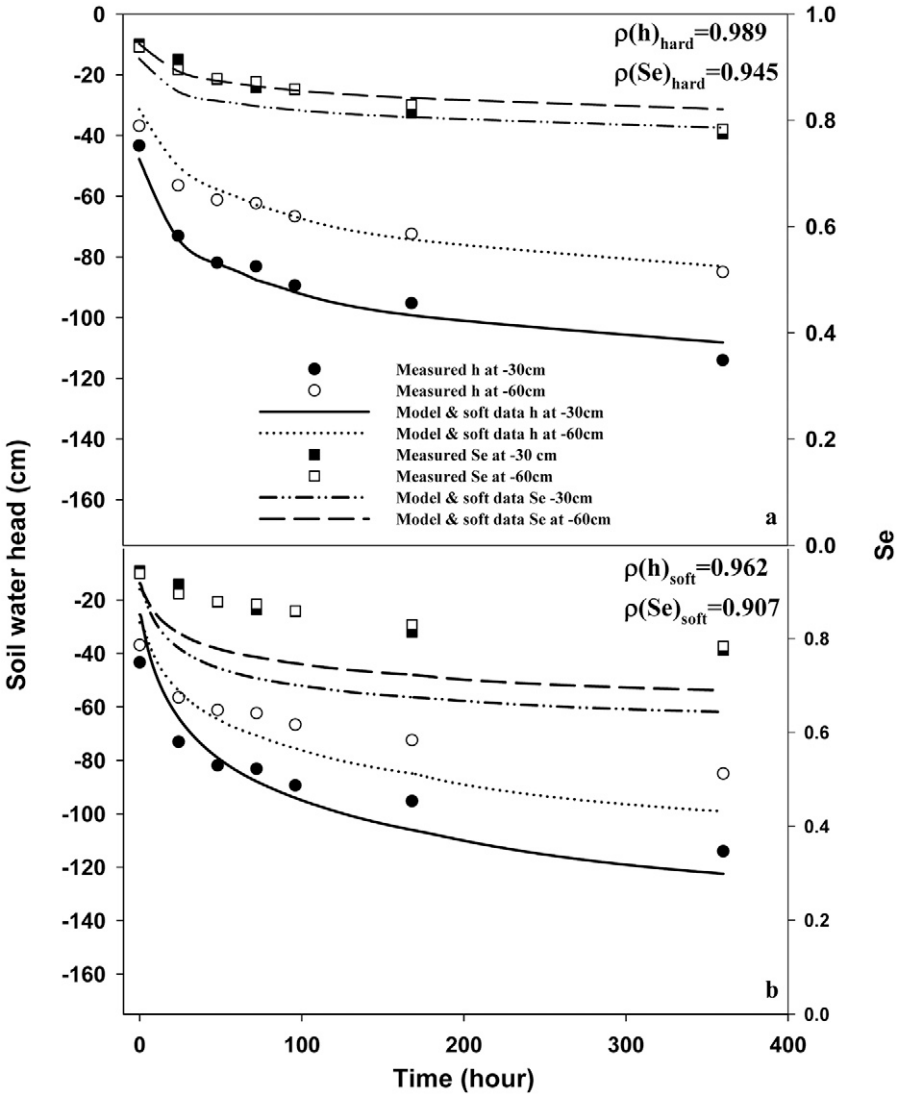

FIG. 12. Simulated (HYDRUS-2D) and measured soil water pressure head (h) and effective water saturation (S_e) from the upper 0 to −90 cm of the profile during a steady-state infiltration and drainage. Time equals zero for steady-state infiltration, and the beginning of the drainage process. The correlation coefficients, ρ, of each parameter are also presented between simulated and field data. Simulations used both (a) hard and (b) soft hydraulic properties given in Table 1.

properties for these simulations were determined from laboratory measurement on undisturbed core samples. The plotted results show two major sections. For values of $q_{surface}$ between 1 and 5 cm d^{-1}, the value of $q_{lateral}/q_{surface}$ increased and was proportional to $q_{surface}$ (section 1). When values of $q_{surface}$ were higher than around 5 cm d^{-1}, the value of $q_{lateral}/q_{surface}$ was around 50% (section 2). Simulation results demonstrate that lateral water flow was always dominated by water flow directly above the sand layer (−70 to −80 cm) for the considered conditions (data not shown). In section 1, water accumulates and increases the hydraulic head directly above the sand layer, and therefore both vertical and lateral flow increased at this location. In section 2, the hydraulic head above the sand layer reaches a value that matches the vertical and horizontal flows for a given surface water infiltration rate. When $q_{surface}$ becomes larger than K_s of the lower silt loam layer (1.6 cm h^{-1}) and the clay lenses (0.018 cm h^{-1}) then water may also be diverted laterally along the bottom of the sand layer due to the significantly higher value of K_s (71.2 cm h^{-1}).

Summary and Conclusions

Field-scale flow and transport studies are frequently conducted to assess and quantify a variety of environmental and agricultural scenarios. The selection and characterization of hydraulic properties (relationships between water pressure, water content, and hydraulic conductivity) at such sites is frequently hampered by heterogeneity of these properties. In this work we presented a multitiered approach to use both hard and soft data in conjunction with pedotransfer functions, interpolation algorithms, and numerical modeling to characterize the hydraulic properties at two 5- by 5-m field plots to a depth of −220 cm.

Relatively easy to measure hard data and more abundant soft data were used to provide initial estimates of soil textural properties at this experimental site. In particular, measurements of electromagnetic induction were used to select the location of the field experimental site in a region with "relatively uniform" soil textural properties. Pictures of excavated soil profiles and approximate particle-size distribution information (laser light scattering) from soil core samples were used to develop an initial conceptual model for the soil stratigraphy. Published pedotransfer functions were then used to predict hydraulic properties from the particle-size distribution and bulk density data.

An interpolation algorithm (nearest neighbor) was used in conjunction with this soft data to quantify spatial variability in the hydraulic properties at this site. The lower portion of the soil profile was found to be very heterogeneous from a depth of −70 to −220 cm, but this region also had persistently high water contents due to the presence of a shallow water table at −220 cm. In this region, spatial variability in saturated conductivity was characterized (i) by determining the effective vertical hydraulic conductivity, and (ii) by developing a three-dimensional representation of the conductivity field. The most appropriate approach for quantifying heterogeneity will likely depend on the questions that need to be answered for a particular application. For example, when considering water quantity problems, the effective vertical conductivity approach is likely to be sufficiently accurate. Conversely, water quality problems such as nitrogen fate and pathogen transport will likely require the more detailed deterministic or stochastic representations of the three-dimensional hydraulic properties.

Hard data were used to better quantify the magnitude of the hydraulic properties at predetermined locations in this plot using both laboratory (multistep outflow, pressure plate, and constant head permeameter techniques on undisturbed cores) and field (instantaneous profile method) measurements. Selection of the sampling location and frequency was guided by the more

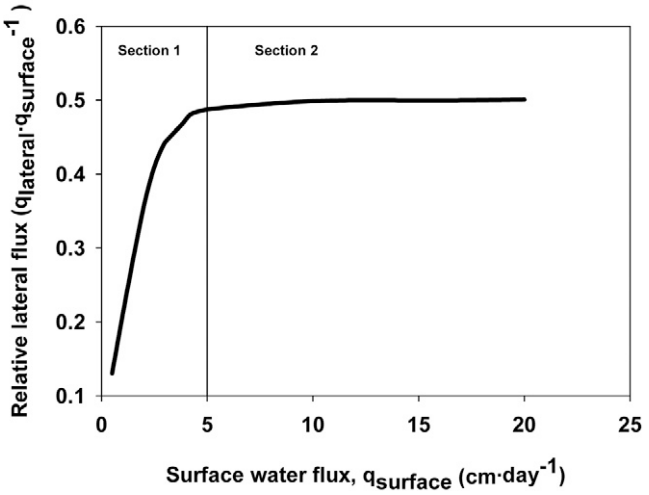

FIG. 13. A plot of the ratio of the simulated lateral water flux through the plot's upper profile to the vertical surface water flux ($q_{lateral}\, q_{surface}^{-1}$) as a function of $q_{surface}$. Hydraulic properties for these simulations were determined from laboratory measurement on undisturbed core samples.

abundant soft data, which was used to identify the different layers and textures in the profile. Despite differences in the measurement scale and technique, measurements of hydraulic properties in the field and on undisturbed core samples were typically very consistent when compared on the basis of effective water saturation. When comparing these measurements in terms of volumetric water content, significant differences were probably because of air entrapment and voids at the core perimeter.

Comparison between measured (hard data) and estimated (soft data) hydraulic properties from several locations in the field suggests that soft data provides a reasonable prediction of soil textural characteristics, but that the specific magnitude of the hydraulic properties are only approximately predicted. Hence, soft data may likely be used to infer trends in spatial variability in soil textural properties, but not to deterministically simulate water flow at the site. Observed and simulated steady-state water infiltration and redistribution in the relatively uniform upper soil profile (0 to −70 cm) support this statement. In this case, simulations that used measured (hard data) hydraulic properties as model input provided a better agreement of observed water flow and drainage. Nevertheless, simulations that used the soft-data-derived hydraulic properties simulations did capture the general water flow behavior and trends. Numerical modeling in conjunction with measured hydraulic properties also proved to be an effective tool to gain additional insight on field scale water flow. For example, we used numerical simulations to quantify the influence of water application rate on the lateral water flux at a location of pronounced soil textural discontinuity in the field at a depth of −70 to −80 cm.

This paper demonstrates the use of different data sources and tools to characterize a field site for flow and transport studies. Integration of both soft and hard data, interpolation algorithms, and numerical modeling was needed to provide a realistic representation of the water flow at our field site. It is likely that other attempts to deterministically predict water flow and contaminant transport in the field will require such a multitiered approach.

Acknowledgments

This research was supported by the 206 Manure and Byproduct Utilization Project of the USDA-ARS and an interagency agreement with the EPA (IAG # DW-12-92189901-0). Although this work has been supported by USDA and EPA, it has not been subjected to Agency review and does not necessarily reflect the views of the Agency, and no official endorsement should be inferred. Similarly, mention of trade names and company names in this manuscript does not imply any endorsement or preferential treatment by USDA or EPA. We would also like to acknowledge the efforts of Yadata F. Tadassa, Michael Troung, Devin Rippner, Mai Lingh Nguyen, and Alan Nguyen in helping to conduct the studies outlined in this paper. We would also like to acknowledge the essential collaboration of Bruce Scott on this project.

References

Abbaspour, K., R. Kasteel, and R. Schulin. 2000. Inverse parameter estimation in a layered unsaturated field soil. Soil Sci. 165:109–123.

Arya, L.M., F.J. Leij, M.Th. van Genuchten, and P.J. Shouse. 1999. Scaling parameter to predict the soil water characteristic from particle-size distribution data. Soil Sci. Soc. Am. J. 63:510–519.

Baker, F.G., P.L.M. Veneman, and J. Bouma. 1974. Limitations of the instantaneous profile method for field measurement of unsaturated hydraulic conductivity. Soil Sci. Soc. Am. Proc. 38:885–888.

Baker, G.S., C. Schmeissner, D.W. Steeples, and R.G. Plumb. 1999. Seismic reflections from depths of less than two meters. Geophys. Res. Lett. 26:279–282.

Birkeland, P.W. 1984. Soils and geomorphology. Oxford Univ. Press, Inc., Oxford, UK.

Blake, G.R., and K.H. Hartage. 1986. Bulk density. p. 363–375. *In* A. Klute (ed.) Methods of soil analysis. Part 1. Physical and mineralogical methods. SSSA Book Ser. 5. ASA and SSSA, Madison, WI.

Bower, H. 1986. Intake rate. Cylinder infiltrometer. p. 825–843. *In* A. Klute (ed.) Methods of soil analysis. Part 1. Physical and mineralogical methods. SSSA Book Ser. 5. ASA and SSSA, Madison, WI.

Bradford, S.A., E. Segal, W. Zheng, Q. Wang, and S.R. Hutchins. 2008. Reuse of CAFO wastewater on agricultural lands. J. Environ. Qual. (in press).

Brooks, R.H., and A.T. Corey. 1964. Hydraulic properties of porous media. Hydrology Papers, No. 3. Colorado State Univ., Fort Collins.

Cameron, K.C., D.E. Harrison, N.P. Smith, and C.D.A. McLay. 1990. A method to prevent edge-flow in undisturbed soil cores and lysimeters. Aust. J. Soil Res. 28:879–886.

Corwin, D.L. 2005. Geospatial measurements of apparent soil electrical conductivity for characterizing soil spatial variability. p. 639–672. *In* J. Álvarez-Benedí and R. Muñoz-Carpena (ed.) Soil-water-solute process characterization: An integrated approach. CRC Press, Boca Raton, FL.

Corwin, D.L., and S.M. Lesch. 2003. Application of soil electrical conductivity to precision agriculture: Theory, principles, and guidelines. Agron. J. 95:455–471.

Corwin, D.L., and S.M. Lesch. 2005a. Apparent soil electrical conductivity in agriculture. Comput. Electron. Agric. 46:11–43.

Corwin, D.L., and S.M. Lesch. 2005b. Characterizing soil spatial variability with apparent soil electrical conductivity I. Survey protocols. Comput. Electron. Agric. 46:103–133.

Daily, W., A. Ramirez, A. Binley, and D. LeBrecque. 2004. Electrical resistance tomography. Leading Edge 23:438–442.

Dane, J.H., and J.W. Hopmans. 2002. Water retention and storage. p. 671–720. In J.H. Dane and G.C. Topp (ed.) Methods of soil analysis. Part 4. Physical methods. SSSA, Madison, WI.

Davis, J.L., and A.P. Annan. 1989. Ground-penetrating radar for high-resolution mapping of soil and rock stratigraphy. Geophys. Prospect. 37:531–551.

Eching, S.O., J.W. Hopmans, and O. Wendroth. 1994. Unsaturated hydraulic conductivity from transient multistep outflow and soil water pressure data. Soil Sci. Soc. Am. J. 58:687–695.

Eshel, G., G.J. Levy, U. Mingelgrin, and M.J. Singer. 2004. Critical evaluation of the use of laser diffraction for particle-size distribution analysis. Soil Sci. Soc. Am. J. 68:736–743.

Flint L.E., and A.L. Flint. 2002. Porosity. p. 241–254. In J.H. Dane and G.C. Topp (ed.) Methods of soil analysis. Part 4. Physical methods. SSSA, Madison, WI.

Flühler, H., M.S. Ardakani, and L.H. Stolzy. 1976. Error propagation in determining hydraulic conductivities from successive water content and pressure head profiles. Soil Sci. Soc. Am. J. 40:830–836.

Gee, G.W., and J.W. Bauder. 1986. Particle-size analysis. p. 383–411. *In* A. Klute (ed.) Methods of soil analysis. Part 1. Physical and mineralogical methods. SSSA Book Ser. 5. ASA and SSSA, Madison, WI.

Goovaerts, P. 1999. Geostatistics in soil science: State-of-the-art and perspectives. Geoderma 89:1–45.

Green, R.E., L.R. Ahuja, and S.K. Chong. 1986. Hydraulic conductivity, diffusivity, and sorptivity of unsaturated soils: Field methods. p. 771–798. *In* A. Klute (ed.) Methods of soil analysis. Part 1. Physical and mineralogical methods. SSSA Book Ser. 5. ASA and SSSA, Madison, WI.

Grossman, R.B., and T.G. Reinsch. 2002. Bulk density and linear extensibility. p. 201–228. In J.H. Dane and G.C. Topp (ed.) Methods of soil analysis. Part 4. Physical methods. SSSA, Madison, WI.

Grote, K., S. Hubbard, and Y. Rubin. 2003. Field-scale estimation of volumetric water content using ground-penetrating radar ground wave techniques. Water Resour. Res. 39(11), 1321, doi:10.1029/2003WR002045.

Hillel, D. 1980. Fundamentals of soil physics. Academic Press, San Diego, CA.

Hillel, D. 1998. Environmental soil physics. Academic Press, San Diego, CA.

Hills, R.G., P.J. Wierenga, D.B. Hudson, and M.R. Kirkland. 1991. The second Las Cruces trench experiment: Experimental results and two-dimensional flow predictions. Water Resour. Res. 27:2707–2718.

Hopmans, J.W., D.R. Nielsen, and K.L. Bristow. 2002. How useful are small-scale soil hydraulic property measurements for large-scale vadose zone modeling? p. 247–258. *In* P.A.C. Raats, D. Smiles, and A.W. Warrick (ed.) Environmental mechanics: Water, mass and energy transfer in the biosphere. Geophysical Monogr. 129. Am. Geophys. Union, Washington, DC.

Hou, Z.S., and Y. Rubin. 2005. On minimum relative entropy concepts and prior compatibility issues in vadose zone inverse and forward modeling. Water Resour. Res. 41:W12425, doi:10.1029/2005WR004082.

Hubbard, S.S., J.S. Chen, J. Peterson, E.L. Majer, K.H. Williams, D.J. Swift, B. Mailloux, and Y. Rubin. 2001. Hydrogeological characterization of the South Oyster Bacterial Transport Site using geophysical data. Water Resour. Res. 37:2431–2456.

Huisman, J.A., S.S. Hubbard, J.D. Redman, and A.P. Annan. 2003. Measuring soil water content with ground penetrating radar: A review. Vadose Zone J. 2:476–491.

Inman, D.J., R.S. Freeland, J.T. Ammons, and R.E. Yoder. 2002. Soil investigations using electromagnetic induction and ground-penetrating radar in southwest Tennessee. Soil Sci. Soc. Am. J. 66:206–211.

Jury, W.A. 1985. Spatial variability of soil physical parameters in solute migration: A critical literature review. EPRI EA-4228, Research Project 2485-6. RPRI, Palo Alto, CA.

Jury, W.A., and R. Horton. 2004. Soil physics. John Wiley & Sons, Hoboken, NJ.

Klute, A. 1986. Water retention: Laboratory methods. p. 635–662. *In* A. Klute (ed.) Methods of soil analysis. Part 1. Physical and mineralogical methods. SSSA Book Ser. 5. ASA and SSSA, Madison, WI.

Klute, A., and C. Dirksen. 1986. Hydraulic conductivity and diffusivity: Laboratory methods. p. 687–734. *In* A. Klute (ed.) Methods of soil analysis. Part 1. Physical and mineralogical methods. SSSA Book Ser. 5. ASA and SSSA, Madison, WI.

Kowalsky, M.B., S. Finsterle, J. Peterson, S. Hubbard, Y. Rubin, E. Majer, A. Ward, and G. Gee. 2005. Estimation of field-scale soil hydraulic and dielectric parameters through joint inversion of GPR and hydrological data. Water Resour. Res. 41:W11425, doi:10.1029/2005WR004237.

Kowalsky, M.B., S. Finsterle, and Y. Rubin. 2004. Estimating flow parameter distributions using ground-penetrating radar and hydrological measurements during transient flow in the vadose zone. Adv. Water Resour. 27:583–599.

Kutilek, M., and D.R. Nielsen. 1994. Field soil heterogeneity. p. 246–272. *In* M. Kutilek and D.R. Nielsen (ed.) Soil hydrology. Catena-Verlag, Reiskirchen, Germany.

Lagerwerff, J.V., F.S. Nakayama, and M.H. Frere. 1969. Hydraulic conductivity related to porosity and swelling of soil. Soil Sci. Soc. Am. Proc. 33:3–11.

Lehmann, F., and P. Ackerer. 1997. Determining soil hydraulic properties by inverse method in one-dimensional unsaturated flow. J. Environ. Qual. 26:76–81.

Lunt, I.A., S.S. Hubbard, and Y. Rubin. 2005. Soil moisture content estimation using ground-penetrating radar reflection data. J. Hydrol. 307:254–269.

Mohanty, B.P., M.D. Ankeny, R. Horton, and R.S. Kanwar. 1994. Spatial variability of hydraulic conductivity measured by disc infiltrometer. Water Resour. Res. 30:2489–2498.

Mualem, Y. 1976. A new model for predicting the hydraulic conductivity of unsaturated porous media. Water Resour. Res. 12:513–522.

Nielsen, D.R., J.W. Biggar, and K.T. Erh. 1973. Spatial variability of field-measured soil-water properties. Hilgardia 42:215–259.

Rajkai, K., and G. Varallyay. 1992. Estimating soil water retention from simpler properties by regression techniques. p. 417–426. *In* M. Th. van Genuchten et al (ed.) Proc. Int. Worksh. on Indirect methods of estimating the hydraulic properties of unsaturated soils. Univ. of California, Riverside. 11–13 Oct. 1989. U.S. Salinity Lab. and Dep. Soil and Environ. Sci., Riverside, CA.

Reginato, R.J., and C.H.M. van Bavel. 1962. Pressure cell for soil cores. Soil Sci. Soc. Am. Proc. 26:1–3.

Reynolds, W.D., B.T. Bowman, R.R. Brunke, C.F. Drury, and C.S. Tan. 2000. Comparison of tension infiltrometer, pressure infiltrometer, and soil core estimates of saturated hydraulic conductivity. Soil Sci. Soc. Am. J. 64:478–484.

Reynolds, W.D., and D.E. Elrick. 1991. Determination of hydraulic conductivity using a tension infiltrometer. Soil Sci. Soc. Am. J. 55:633–639.

Rhoades, J.D. 1993. Electrical conductivity methods for measuring and mapping soil salinity. Adv. Agron. 49:201–251.

Richards, L.A. 1965. Physical condition of water in soil. p. 128–152. *In* C.A. Black (ed.) Methods of soil analysis. Part 1. Agron. Monogr. 9. ASA and SSSA, Madison, WI.

Romano, N. 1993. Use of an inverse method and geostatistics to estimate soil hydraulic conductivity for spatial variability analysis. Geoderma 60:1–4.

Russo, D., and E. Bresler. 1981. Soil hydraulic properties as stochastic processes: I. An analysis of field spatial variability. Soil Sci. Soc. Am. J. 45:682–687.

Schaap, M.G., F.J. Leij, and M.Th. van Genuchten. 2001. ROSETTA: A computer program for estimating soil hydraulic parameters with hierarchical pedotransfer functions. J. Hydrol. 251:163–176.

Scheidegger, A.E. 1957. The physics of flow through porous media. Macmillan, New York.

Šimůnek, J., K. Huang, M. Šejna, and M.Th. van Genuchten. 1999. The HYDRUS-2D software package for simulating two-dimensional movement of water, heat and multiple solutes in variably-saturated media. Version 2.0. IGWMC-TPS-53, Int. Ground Water Modeling Center, Colorado School of Mines, Golden.

Šimůnek, J., M.Th. van Genuchten, M.M. Gribb, and J.W. Hopmans. 1998. Parameter estimation of unsaturated soil hydraulic properties from transient flow processes. Soil Tillage Res. 47:27–36.

Thomasson, M.J., P.J. Wierenga, and T.P.A. Ferre. 2006. A field application of the scaled-predictive method for unsaturated soil. Vadose Zone J. 5:1093–1110.

Tuli, A., J.W. Hopmans, D.E. Rolston, and P. Moldrup. 2005. Comparison of air and water permeability between disturbed and undisturbed soils. Soil Sci. Soc. Am. J. 69:1361–1371.

Ünlü, K., D.R. Nielsen, J.W. Biggar, and F. Morkoc. 1990. Statistical parameters characterizing the spatial variability of selected soil hydraulic properties. Soil Sci. Soc. Am. J. 54:1537–1547.

van Genuchten, M.Th. 1980. A closed-form equation for predicting the hydraulic conductivity of unsaturated soils. Soil Sci. Soc. Am. J. 44:892–898.

van Genuchten, M.Th., F.J. Leij, and S.R. Yates. 1991. The RETC code for quantifying the hydraulic functions of unsaturated soils. Rep. EPA/600/2-91/065. R.S. Kerr Environmental Research Lab., USEPA, Ada, OK.

Vereecken, H., R. Kasteel, J. Vanderborght, and T. Harter. 2007. Upscaling hydraulic properties and soil water flow processes in heterogeneous soils: A review. Vadose Zone J. 6:1–28.

Watson, K.K. 1966. An instantaneous profile method for determining the hydraulic conductivity of unsaturated porous materials. Water Resour. Res. 2:709–715.

Wierenga, P.J., R.G. Hills, and D.B. Hudson. 1991. The Las Cruces trench site: Characterization, experimental results, and one-dimensional flow predictions. Water Resour. Res. 27:2695–2705.

Zhang, Z.F., A.L. Ward, and G.W. Gee. 2004. A parameter scaling concept for estimating field-scale hydraulic functions of layered soils. J. Hydraul. Res. 42:93–103.